Dalton Transactions

ROYAL SOCIETY OF CHEMISTRY

PAPER

View Article Online
View Journal

Cite this: DOI: 10.1039/d5dt02352a

^{68}Ga radiolabeling strategies in Pt(IV)-deferoxamine scaffolds for potential theranostic application

Giulia Ferrari,†[a] Ines Lopez-Martinez,†[b,d] Mohamad Saqawa,[c,g] Eithne Demspey,[a] Thomas Wanek,[d] Irena Pashkunova-Martic,[d,e] Silvia Panseri,[c] Marcus Hacker,[b] Monica Montesi,*[c] Claudia Kuntner*[d,e] and Diego Montagner*[a,f]

Since the discovery of cisplatin's anticancer activity and its clinical approval in 1978, substantial efforts have focused on improving its physiological stability and minimizing off-target toxicity. One promising strategy has been the development of Pt(IV) complexes, which act as redox-activated prodrugs with improved pharmacological profiles compared to Pt(II) drugs. In this study, we present the synthesis of three novel Pt(IV) complexes bearing a pendant deferoxamine (DFO) chelator, designed for theranostic application, combining therapeutic activity with radiometal labeling for positron emission tomography (PET) imaging. Platinum-based drugs are still the gold standard therapy for osteosarcoma but the limited utility and the resistance mechanisms indicate an urgent need for new approaches. *In vitro* studies demonstrated that these complexes are efficiently internalized by osteosarcoma cells and exhibit minimal toxicity toward healthy MDCK.2 kidney cells, indicating a favorable safety profile. Radiolabeling with Gallium-68 was achieved under mild conditions, yielding stable radiotracers in various biological media after 1 h incubation. This study represents one of the first demonstrations of Pt(IV) theranostic agents suitable for PET imaging, enabling future investigations of Pt(IV) biodistribution profiles that go beyond traditional therapeutic evaluations.

Received 1st October 2025,
Accepted 30th November 2025

DOI: 10.1039/d5dt02352a

rsc.li/dalton

Introduction

Platinum(II)-based drugs have played a central role in medicine since the discovery of the antitumor activity of cisplatin in 1978. These agents remain among the most widely used chemotherapeutics for the treatment of various cancers, including testicular, ovarian, lung, bladder, breast and osteosarcoma.[1] Beyond oncology, platinum complexes have also shown potential against bacterial and viral infections,[2,3] highlighting their versatile bioactivity and promising increasing interest in their development as multifunctional platforms.

Despite their clinical success, Pt(II) drugs suffer from severe dose-dependent side effects and the emergence of resistance mechanisms that reduce the therapeutic efficacy.[4] To address these limitations, Pt(IV) prodrugs have been extensively explored over the past two decades as promising alternatives.[5,6] These Pt(IV) derivatives undergo *in vivo* intracellular reduction, particularly in the hypoxic tumor microenvironment, releasing their axial ligands and generating the corresponding cytotoxic Pt(II) species.[7] The extra coordination sites allow numerous possibilities for introducing further moieties in the axial position, obtaining multifunctional Pt(IV) agents. The additional functionalities can serve various roles, for example as passive uptake enhancers, targeting agents, or molecules to facilitate the conjugation to carrier systems. Additionally, they can be bioactive drugs with new modes of action, synergistically enhancing the pharmacological profile.[5] Beyond purely therapeutic optimization, axial functionalization of Pt-based drugs offers the opportunity to incorporate diagnostic tools,[8] paving the way for radiolabeled Pt(IV) systems that can be used to investigate drug distribution, stability and biological fate – key parameters for future theranostic development.

Among available radionuclides, ^{68}Ga is a particularly attractive radioisotope for oncological PET imaging, owing to its suitable half-life (68 min), which is long enough to accommodate radiolabeling, quality assurance and sufficient circulation

[a]*Department of Chemistry, Maynooth University, Maynooth, Ireland. E-mail: diego.montagner@mu.ie*
[b]*Division of Nuclear Medicine, Department of Biomedical Imaging and Image-Guided Therapy, Medical University of Vienna, Vienna, Austria*
[c]*Institute of Science, Technology and Sustainability for Ceramics (ISSMC) – National Research Council (CNR), Faenza, RA, Italy. E-mail: monica.montesi@issmc.cnr.it*
[d]*Preclinical Imaging Lab (PIL), Department of Biomedical Imaging and Image-Guided Therapy, Medical University of Vienna, Vienna, Austria. E-mail: claudia.kuntner@meduniwien.ac.at*
[e]*Research Platform Medical Imaging (RPMI), Medical University of Vienna, Vienna, Austria*
[f]*Kathleen Londsdale Institute for Human Health Research, Maynooth University, Ireland*
[g]*Department of Chemical, Biological, Pharmaceutical, and Environmental Sciences, University of Messina, Messina, Italy*
†These authors contributed equally.

time for target accumulation, while being short enough to minimize patient radiation exposure. Moreover, the availability of ^{68}Ga as a generator-derived radionuclide ensures broad applicability of labeled compounds, as a cyclotron facility for local radionuclide production is not required.

Deferoxamine (DFO) is a bacterial siderophore clinically used as an iron chelator for the treatment of iron overload[9] that has also emerged as the benchmark chelator for Zirconium-89 in immunoPET applications.[10] Interestingly, while DFO is most commonly associated with ^{89}Zr, it also forms highly stable complexes with ^{68}Ga. This is due to the similar coordination chemistry of Fe^{3+} and Ga^{3+} both are hard Lewis acids with comparable ionic radio and a preference for octahedral, hexadentate coordination environments. As a result, radiolabeling with ^{68}Ga can be performed under mild (*e.g.* 35 °C) and fast (*e.g.* reaction times 5–10 min) conditions, highlighting the versatility of DFO and underscoring its potential for applications where short-lived isotopes are advantageous.

As a proof-of-concept, we selected osteosarcoma, the most common primary malignant bone tumor in adolescents and young adults,[11] as a relevant model to explore the theranostic potential of Pt(IV)-DFO conjugates. Platinum(II)-based drugs, such as cisplatin, are widely used in chemotherapy protocols for osteosarcoma, often in combination with other agents to exploit different mechanisms of action.[12,13] Although the combination of multi-agent chemotherapy and surgery increased the five-year survival rate from 15–20% in the 1970s to 50–70% in the 1980s,[14] outcomes have remained largely unchanged over the past three decades. Moreover, no specific diagnostic radiotracer has yet been approved for osteosarcoma, and current clinical imaging still relies primarily on 2-deoxy-2-[^{18}F] fluoroglucose ([^{18}F]-FDG).[15–17]

Here, we report the synthesis, characterization, and radiolabeling protocols of a series of Pt(IV)-based complexes derived from the clinically approved drugs cisplatin and oxaliplatin, functionalized with DFO to enable radiolabeling for theranostic applications. To the best of our knowledge, three prior examples of Pt(IV)-DFO conjugates have been described,[18–20] including the study by Harringer *et al.*[19] on carboplatin-based derivatives, that reports interaction studies with non-radioactive metal ions and the most recent work by Kraihammer *et al.*[20] that evaluates related complexes for application in *Aspergillus fumigatus*. Building on this foundation, our study focuses on the synthesis of cisplatin- and oxaliplatin-based conjugates (Fig. 1), allowing a direct comparison of these clinically relevant scaffolds within the context of Pt(IV) theranostic prodrugs in osteosarcoma.

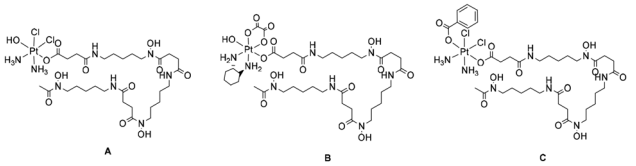

Fig. 1 Structure of the three DFO-functionalized Pt(IV) complexes.

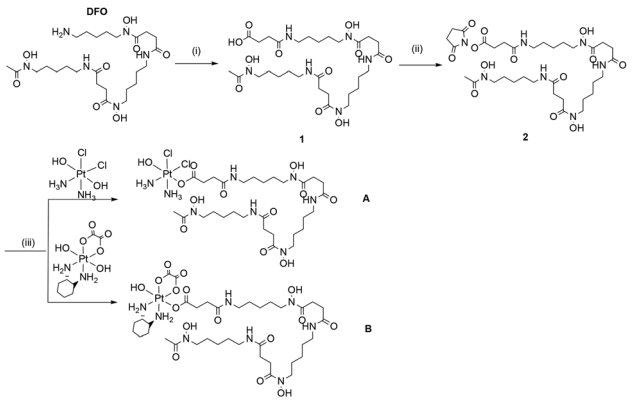

Scheme 1 Synthesis of complexes **A** and **B**: (i) DFO mesylate, succinic anhydride, dry pyridine, r.t, 24 h; (ii) TSTU, DIPEA, DMSO, r.t., 2 h; (iii) Pt (IV), DMSO, 50 °C, 72 h.

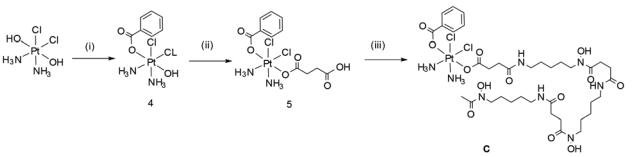

Scheme 2 Synthesis of complex **C**: (i) oxoplatin, benzoic anhydride, DMSO, r.t, 12 h; (ii) succinic anhydride, DMSO, 50 °C, 24 h; (iii) DFO mesylate, TBTU, TEA, DMF, 35 °C, 12 h.

Results and discussion

Synthesis

The three DFO-Pt(IV) complexes **A**, **B** and **C** were obtained *via* two different synthetic approaches, as illustrated in Scheme 1 for complexes **A** and **B** and in Scheme 2 for complex **C**. Complexes **A** and **B** are monoadducts with a single axial position functionalized by DFO, while complex **C** contains a benzoyl group in the second axial position, to investigate the effect of a lipophilic ligand on the cellular uptake and complex stability. To enable the coordination of the deferoxamine mesylate (DFO mesylate) to the hydroxyl groups on Pt(IV) complexes, the terminal amine of DFO was functionalized. A succinyl moiety was introduced by reacting DFO-mesylate with succinic anhydride in dry pyridine, obtaining the carboxylic acid derivative (**1**, Scheme 1). The resulting carboxylic acid was then activated with an NHS ester, following a well-established procedure previously applied in our group for the synthesis of Pt (IV) prodrugs.[21,22] However, in this case, the NHS-activation with TSTU (*N*,*N*,*N*′,*N*′-tetra methyl-*O*-(*N*-succinimidyl)uronium tetrafluoroborate) resulted in incomplete conversion to **2**. During esterification, a competing intramolecular cyclization formed a mixture of the desired NHS active ester (compound **2**) and the succinimide by-product (compound **3**, Scheme 1S,

SI).[23] The formation of the by-product was dependent on the amount of triethylamine used. The cyclic compound was unambiguously identified by ^{1}H NMR and mass spectrometry (Fig. 1Sa and b, SI). Optimal conditions for minimizing the formation of **3** were found with 1.2 equivalents of the base. The crude compound **2** was used without further purification and reacted with oxoplatin and dihydroxyoxaliplatin, to produce **A** and **B**, respectively. The final complexes were purified by preparative HPLC, as described in the Experimental section.

To obtain **C**, a preliminary substitution of one of the OH axial group in oxoplatin with a benzoic group was required (**4**, Scheme 2), followed by the substitution of the other hydroxo group in *trans* with the succinic acid to obtain **5**. The last step involved the coupling of the carboxylic acid in **5** with the amine of the deferoxamine mesylate (Scheme 2).[24] This synthetic route avoided the cyclization side reaction described earlier obtaining a pure product. For **A** and **B**, any attempt made to use the same strategy proved unsuccessful.

For radiolabeling, a precursor purity of at least 95% is required, and this was achieved for the three complexes by preparative HPLC (eluent MeCN/H_2O or MeOH/H_2O + 0.1% of TFA).

The final complexes, as well as all the intermediates, were characterized by 1D and 2D multi nuclear NMR (^{1}H, ^{13}C, ^{195}Pt) spectroscopy and mass spectrometry and the purity was assessed by HPLC and elemental analysis (Fig. 2S–8S). The complexes revealed to be stable under physiological conditions for over a month as seen from LC-mass in water solution (Fig. 9S). The pro-drug nature of complexes **A**, **B** and **C** was assessed by LC-MS following the addition of an excess of ascorbic acid to PBS solutions. All complexes underwent nearly complete reduction within 24 hours, with the release of their axial ligands (Fig. 2 and Fig. 10S).[25]

The reduction potentials of the Pt(IV) complexes **A**, **B** and **C** and of the ligand **1** were determined *via* cyclic voltammetry (Fig. 2 and Fig. 10S, 11S), and the results are summarized in Table 1S in SI. The E_p values (labeled as peak II_c) for the irreversible reduction process Pt(IV)/Pt(II) were determined to be −1.33, −1.45 and −1.13 V, for complexes **A**, **B** and **C**, respectively, in line with previously reported Pt(IV) species based on cisplatin and oxaliplatin.[26–28]

Biological evaluation *in vitro*

The anticancer activity of the compounds was tested *in vitro* against two different osteosarcoma cancer cell lines (U2OS and 143B). Moreover, the nephrotoxicity of the complexes was tested *in vitro* in MDCK.2 cells, a Madin–Darby canine kidney cell line, commonly used to study nephrotoxicity, particularly in models involving platinum-induced damage.[29]

Complexes **A**, **B** and **C** displayed a generally lower biological activity compared to cisplatin and oxaliplatin, which were used as positive controls. As expected, after 3 days in both osteosarcoma cell lines, all the complexes did not exert sufficient toxicity to reduce viability by 50%, even at higher concentrations. For this reason, the anticancer activity was assessed by exposing the cells to the complexes and controls for longer periods, up to day 7, in order to obtain IC_{50} values (Table 1 and Fig. 12S).

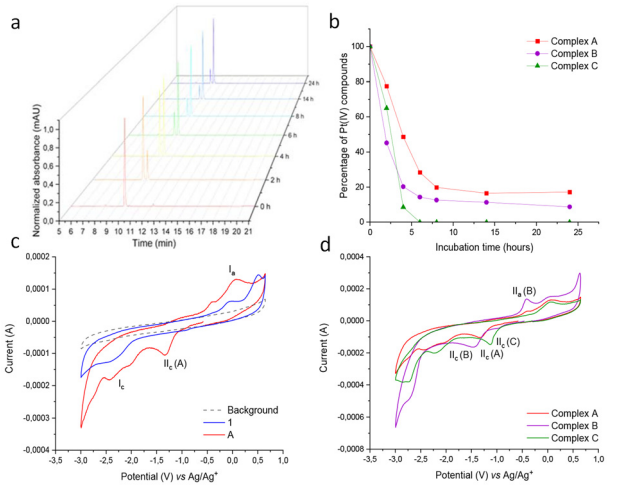

Fig. 2 Reduction of Pt(IV) complexes (0.1 M, PBS buffer, pH 7.4 at 37 °C, 10 eq. of sodium ascorbate, 24 h) and electrochemical characterization using cyclic voltammetry (CV). (a) LC mass chromatograms of the reduction of **A**; (b) percentage of remaining starting complexes after 24 h; (c) CV of complex **A** in comparison to ligand **1** in DMSO; (d) comparative CV of the complexes **A–C** in DMSO.

Complex **B** reduces cell viability below 50% only at 60 μM after 7 days of treatment in both osteosarcoma cell lines; however, that is not sufficient to obtain a good fit for the IC_{50} value. These results are not unexpected, being DFO a biologically innocent hydrophilic ligand that indeed contributes to a lower cellular uptake resulting in a poor anticancer activity. As discussed later, compound **C** with a lipophilic benzyl group in the other axial position shows a higher intracellular internalization and showed the highest cytotoxic activity. A detailed analysis of the cell viability data revealed that complex **C** exerted a stronger toxic effect compared to complexes **A** and **B** in both cell lines. In U2OS cells, treatment with 30 μM of Complex **C** for 7 days significantly reduced cell viability to 12.4 ± 2.0%, showing an effect comparable to that of oxaliplatin, used as a positive control (9.2 ± 0.3%). By contrast, complexes **A** and **B** resulted in higher viability values of 45 ± 3.3% and 70 ± 9.1%, respectively (Fig. 3).

Table 1 IC_{50} (μM) values at day 7 of the complexes **A**, **B**, **C**, cisplatin and oxaliplatin against U2OS, 143B and MDCK.2 cells

	U2OS IC_{50} (95%)	143B IC_{50} (95%)	MDCK.2 IC_{50} (95%)
Cisplatin	2.07 (1.44–2.72)	0.45 (0.437–0.453)	6.64 (0.585–>100)
Oxaliplatin	5.71 (5.05–6.34)	5.09 (4.62–5.32)	>60
Complex **A**	26.5 (22.7–33.0)	19.48 (16.46–25.11)	>60
Complex **B**	[a]	[a]	>60
Complex **C**	16.76 (8.74–>100)	13.74 (9.90–15.29)	>60

[a] Ambiguous fitting.

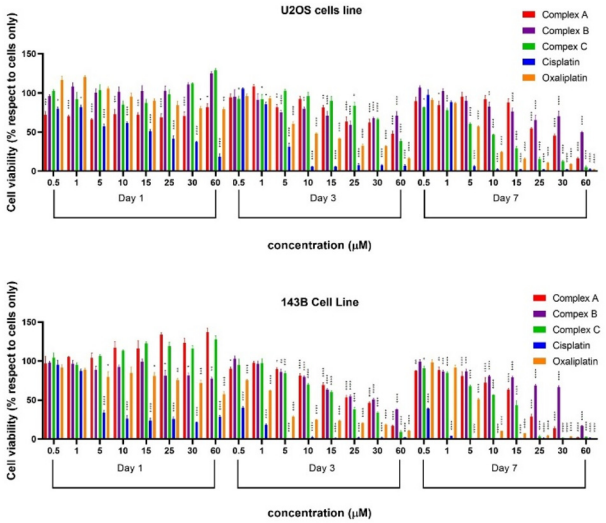

Fig. 3 Screening of complexes **A**, **B** and **C** by MTT assay in U2OS (top) and 143B (bottom) cell viability evaluation (%) mean ± standard error of the mean. Statistical analyses with respect to cells only are reported in the graph, *p* value is *≤0.05, **≤0.01, ***≤0.001 and ****≤0.0001.

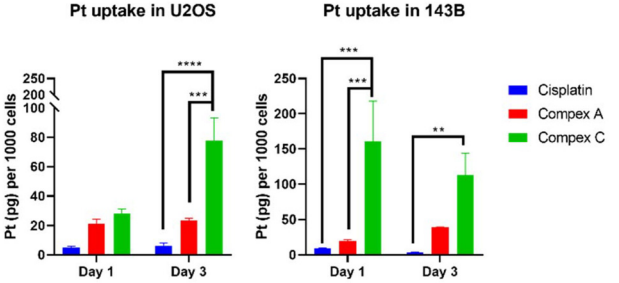

Fig. 4 Cellular uptake of picograms of platinum ions (mean ± standard error) per 1000 cell are reported in the graphs. *p* value **≤0.01, ***≤0.001 and ****≤0.0001.

A similar trend was observed in 143B cells at day 7 with 30 μM treatment, where only complex **C** displayed higher toxicity than oxaliplatin, with viability values of 1.5 ± 0.3% and 3.0 ± 0.3%, respectively (Fig. 3). In this cell line, complexes **A** and **B** at 60 μM exhibited greater toxicity compared to their effects in U2OS cells. Indeed, complexes **A** and **C** produced results comparable to those of cisplatin and oxaliplatin, while complex **B**, although more active in 143B than in U2OS, still resulted in 16.8 ± 0.6% cell viability (Fig. 3 and Fig. 12S). The qualitative analysis of cell morphology confirmed the cytotoxicity results (Fig. 13S).

The analysis in the MDCK.2 cell line revealed very low levels of nephrotoxicity even at high concentrations for all the complexes, with the exception of cisplatin, which showed the expected behaviour.[30] All three complexes in fact maintained high levels of cell viability after 3 days of culture; complex **C**, in particular, showed 75.4 ± 3.7% viability, similar to oxaliplatin but higher compared to all the other compounds tested (Fig. 14S). Due to this low toxic effect and to the growth rate of these cells, it was not possible to perform the MTT assay on day 7, since the cultures became overconfluent, causing interferences that produced unreliable results (Table 1). To shed light on the cytotoxic activity, cellular uptake studies were performed with the most effective complexes **A** and **C**, that are the analogous based on cisplatin with cisplatin used as a positive control (Fig. 4). For this assay, IC_{50} concentrations of each compound were used and the results suggest that the higher activity of complex **C** is due to its greater uptake rate compared to complex **A** (between 50 and 75% higher uptake at day 3 in U2OS and 143B, respectively). Overall, it was observed that in 143B cells the uptake of both complexes was higher compared to U2OS cells, confirming the high activity demonstrated in these cells, while cisplatin uptake was similar in both cell lines. The different behaviors observed between the two osteosarcoma cell lines can be attributed to their well-known differences in genetic complexity, which underline cell-specific biological characteristics (*e.g.*, tumorigenicity, colony-forming ability, invasive/migratory potential, metabolism, and proliferation capacity).[31,32]

Consistent with our expectations, the tested complexes, particularly **C**, which showed the greatest potential, displayed lower anticancer activity than cisplatin while exhibiting higher tolerability in renal cells. This dual profile is especially significant for the development of a theranostic platform, as it highlights the possibility of combining effective antitumor activity with compatibility for simultaneous diagnostic applications.

It is worth noting that coordination of Gallium to DFO could, in principle, affect properties such as lipophilicity, charge, and stability, potentially influencing cytotoxicity. In this study, however, all *in vitro* assays were performed with Ga-free complexes to evaluate the intrinsic properties of the Pt(IV) prodrugs independently of metal coordination.

Radiolabeling

Radiolabeling of complexes **A**, **B** and **C** (15 μM for **A** and **B**, and 14 μM for **C**) with Gallium-68 was successfully achieved in a 10 min reaction time with incorporation yields of 100% and radiochemical purities of 94–97% at the end of synthesis (Fig. 5), under aqueous mild conditions without the need of further purification. Our protocol, adapted from ref. 18, afforded a markedly higher molar activity (25 MBq $nmol^{-1}$) compared to their previously reported value of 1.585 MBq $nmol^{-1}$. As expected, "free" unchelated gallium eluted with the solvent front under the same gradient conditions (Fig. 15S). A minor additional species was consistently observed, identified as [^{68}Ga]-**1** *via* co-elution with cold [Ga]-**1** (Fig. 16Sa–c). This species likely arises from partial ester hydrolysis of the axial ligand under the acidic radiolabeling conditions (pH 4.5).

All [^{68}Ga]-labelled compounds demonstrated high stability in water, PBS, and human blood serum after 1 h (Fig. 17Sa–c, 18Sa–c and 19Sa–c). In contrast, when incubated with human liver microsomes, stability decreased to 19%, 58%, and 78%, indicating degradation into [^{68}Ga]-**1** most likely due to enzy-

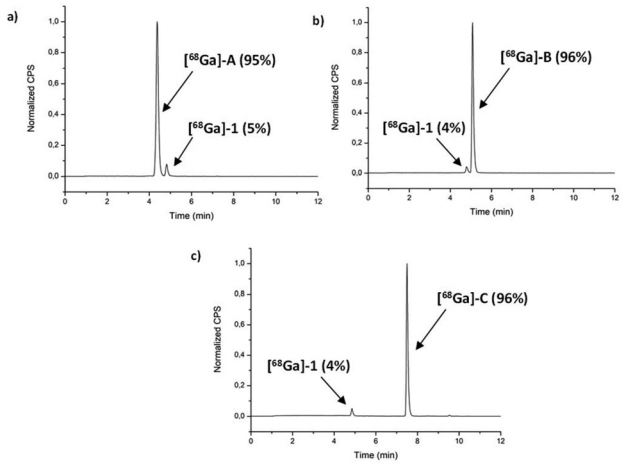

Fig. 5 Radio RP-HPLC chromatograms of (a) [^{68}Ga]-**A** (t_R = 4.4min); (b) [^{68}Ga]-**B** (t_R = 5.0min) and (c) [^{68}Ga]-**C** (t_R = 7.5min). Conditions: 5–30% MeCN/H_2O with 0.1% TFA (v/v), 8 min.

matic cleavage by liver esterases (Fig. 17–19Sd). Notably, ester bond cleavage is an integral part of the theranostic design, as it enables release of the cytotoxic moiety *in vivo*. Nevertheless, considerable efforts have been made to minimize the proportion of [^{68}Ga]-1, since purities of ≥95% are required for diagnostic applications (Fig. 5).

Radio-TLC profiles for [^{68}Ga]-**A–C** and for free [^{68}Ga]Ga^{3+} are reported in Fig. 20S. Moreover, the physicochemical profiles of [^{68}Ga]-**A**, [^{68}Ga]-**B** and [^{68}Ga]-**C** were assessed *via* log *D* (octanol/PBS, pH 7.4) and plasma protein binding studies (Table 2). Compounds **A** and **B** were highly hydrophilic, with log *D* values of −3.7 and −3.0, respectively, while [^{68}Ga]-**C** was more lipophilic (log *D* = −1.4). Interestingly, [^{68}Ga]-**A** exhibited a higher plasma protein binding (71%) than [^{68}Ga]-**B** (51%), despite being more hydrophilic, whereas [^{68}Ga]-**C** showed the highest binding (95%), consistent with its greater lipophilicity. This suggests that factors beyond lipophilicity, such as overall charge distribution or molecular conformation, may influence protein interactions.

Table 2 Chemical purity (CP), ^{68}Ga-labeling purity (RCP), stability tests performed in PBS, human blood serum and human liver microsomes for 1 h, log *D* and plasma protein binding (PPB) of complexes **A**, **B** and **C**

Compound	CP (%)	RCP (%)	Stability tests	Log *D* pH = 7.4	PPB (%)
[^{68}Ga]-**A**	97	94 ± 1	PBS (93%) Blood (90%) Liver (19%)	−3.7 ± 0.2	71 ± 1
[^{68}Ga]-**B**	98	97.2 ± 0.4	PBS (96%) Blood (95%) Liver (58%)	−3.0 ± 0.3	54 ± 1
[^{68}Ga]-**C**	95	95 ± 2	PBS (91%) Blood (84%) Liver (78%)	−1.4 ± 0.1	95 ± 1

Experimental section

A detailed description of the Material and methods and the spectroscopic characterization are reported in the SI.

Synthesis

Cisplatin, oxoplatin, oxaliplatin and dihydroxyoxalyplatin were synthetized as previously reported.[33,34]

Deferoxamine succinic acid (1). Deferoxamine mesylate (0.5 g, 0.76 mmol) was dissolved in dry pyridine (18.4 mL) and succinic anhydride (0.76 g, 7.62 mmol) was added to the solution that was stirred at r.t. for 24 h. 100 mL of NaOH solution (0.15 M) was added and the mixture was stirred at r.t. for a further 16 h. The pH was adjusted to 2 with HCl (12 M) and cooled to 4 °C for 2 h. The precipitate was filtered, washed with 100 mL of HCl (0.01 M), and dried under vacuum (yield: 0.39 g, 77%). ^{1}H-NMR (500 MHz, DMSO-d_6): δ 12.05 (s, 1H, COO*H*) 9.65 (s, 1H, H_3CCONO*H*), 9.60 (s, 2H, COONO*H*), 7.77 (s, 3H, COON*H*), 3.45 (t, *J* = 7.4 Hz, 6H, HONCH_2), 3.00 (q, *J* = 6.6 Hz, 6H, HNCH_2), 2.57 (t, *J* = 7.6 Hz, 4H, HONCOCH_2), 2.40 (t, *J* = 6.5 Hz, 2H, CH_2COOH), 2.28 (m, 6H, HNCOCH_2), 1.96 (s, 3H, CH_3), 1.54–1.44 (m, 6H, HONCH$_2$CH_2), 1.42–1.33 (m, 6H, HNCH$_2$CH_2), 1.26–1.17 (m, 6H, HNCH$_2$CH$_2$CH_2). ^{13}C NMR (126 MHz, DMSO-d_6) δ 173.92 (*C*OOH), 172.02 (HON*C*O), 171.41 (HN*C*O), 170.84 (*C*OCH$_2$CH$_2$COOH), 170.23 (CH$_3$*C*O), 47.13 and 46.84 (HON*C*H$_2$), 38.48 (NH*C*H$_2$), 30.05 and 29.96 (HNCO*C*H$_2$), 29.24 (*C*H$_2$COOH), 28.84 (HNCH$_2$*C*H$_2$), 27.63 (HONCO*C*H$_2$), 26.06 (HONCH$_2$*C*H$_2$), 23.53 (HNCH$_2$CH$_2$*C*H$_2$), 20.39 (CH$_3$). HR-MS: calculated mass for (M + H)$^+$: 661.3964, found 661.38 [M + H]$^+$.

2,5-Dioxopyrrolidin-1-yl (deferoxamine-succinate) (2). 0.05 g of **1** (0.075 mmol) was added to a flask containing molecular sieves and TSTU (0.025 g, 0.083 mmol) under N_2. 4.5 mL of dry DMSO and 15 μL of anhydrous triethylamine were added and the reaction was stirred at r.t. for 2 h. Molecular sieves were removed by filtration and the DMSO was evaporated by lyophilization. The residue was washed sequentially with dichloromethane and diethyl ether, dried under vacuum, and used for the last step without further purification (yield: 0.053 g, 85%). ^{1}H-NMR (500 MHz, DMSO-d_6): δ 9.65 (s, 1H, H_3CCONO*H*), 9.60 (s, 2H, COONO*H*), 7.90 (t, *J* = 5.4 Hz, 1H, NH_{succ}), 7.77 (s, 3H, COON*H*), 3.45 (t, *J* = 7.4 Hz, 6H, HONCH_2), 3.00 (q, *J* = 6.6 Hz, 6H, HNCH_2), 2.79 (s, 4H, CH_{2succ}) 2.57 (t, *J* = 7.6 Hz, 4H, HONCOCH_2), 2.40 (t, *J* = 6.5 Hz, 2H, CH_2COOH), 2.28–2.25 (m, 6H, HNCOCH_2), 1.96 (s, 3H, CH_3), 1.54–1.44 (m, 6H, HONCH$_2$CH_2), 1.42–1.33 (m, 6H, HNCH$_2$CH_2), 1.26–1.17 (m, 6H, HNCH$_2$CH$_2$CH_2). ^{13}C NMR (126 MHz, DMSO-d_6) δ 171.96 (HON*C*O), 171.30 (HN*C*O), 170.13 (*C*OCH$_2$CH$_2$COO and *C*O$_{succ}$), 169.40 (HN*C*O$_{succ}$), 168.67 (CH$_3$*C*O) 47.08 and 46.79 (HON*C*H$_2$), 38.54 and 38.42 (NH*C*H$_2$), 29.90 (HNCO*C*H$_2$), 29.24 (*C*H$_2$CH$_2$COOH), 28.81 (HNCH$_2$*C*H$_2$), 27.56 (HONCO*C*H$_2$), 26.02 (HONCH$_2$*C*H$_2$), 25.97 (CH$_2$COO), 25.42 (*C*H$_{2suc}$) 23.49 (HNCH$_2$CH$_2$*C*H$_2$), 20.35 (CH$_3$). LC-MS: calculated mass for (M + H)$^+$: 758.3858, found 758.39.

***cis*,*cis*,*trans*-[Pt(NH$_3$)$_2$(Cl)$_2$(OH)-deferoxamine succinate] (A).** 0.05 g of **2** (0.066 mmol) were dissolved in 4 mL of dry DMSO

and the solution was added dropwise to a suspension of *cis*,*cis*,*trans*-$[Pt(NH_3)_2Cl_2(OH)_2]$ (0.023 g, 0.069 mmol) in 1 mL of DMSO. The solution was stirred at r.t. for 48 h in the dark at 40 °C, resulting in a light-yellow suspension. After filtration through cotton wool, the DMSO was evaporated by lyophilization and the residue was washed with methanol (2 × 5 mL), dichloromethane (5 mL) and diethyl ether (2 × 5 mL) and dried under reduced pressure. The residue was purified *via* isocratic preparative reversed phase high-performance liquid chromatography (RP-HPLC), (C18 X-Bridge) using MeCN/H_2O 15 : 85 with 0.1% TFA as the eluent over 12 min. The product eluted at 7.6 min, affording the pure compound as a pale-yellow powder (yield: 0.015 g, 23%). ^{1}H NMR (500 MHz, DMSO-d_6) δ 9.66 (s, 1H, $H_3CCONOH$), 9.62 (s, 2H, $COONOH$), 7.81–7.76 (m, 3H, NH), 6.10 (t, J_{N-H} = 51.4 Hz, 6H, NH_3), 3.45 (t, J = 7.4 Hz, 6H, $HONCH_2$), 3.00 (q, J = 6.6 Hz, 6H, $HNCH_2$), 2.57 (t, J = 7.1 Hz, 4H, $HONCOCH_2$), 2.42 (t, J = 7.4 Hz, 2H, CH_2COOH), 2.28–2.25 (m, 6H, $HNCOCH_2$), 1.96 (s, 3H, CH_3), 1.54–1.45 (m, 6H, $HONCH_2CH_2$), 1.43–1.33 (m, 6H, $HNCH_2CH_2$), 1.26–1.13 (m, 6H, $HNCH_2CH_2CH_2$). ^{13}C NMR (125 MHz, DMSO-d_6) δ 180.02 (COO–Pt), 171.99 (HONCO), 171.40 ($NHCO_{succ}$), 171.34 (CONH) 170.17 ($COCH_3$), 47.10 and 46.80 ($HONCH_2$), 38.43 ($HNCH_2$), 31.65 (CH_2COO–Pt), 30.69 (CH_2CH_2COO–Pt), 29.92 (CH_2CONH), 28.83 ($HNCH_2CH_2$), 27.58 ($HONCOCH_2$), 26.05 ($HONCH_2CH_2$), 23.51 ($HNCH_2CH_2CH_2$), 20.37 (CH_3). ^{195}Pt{^{1}H} NMR (108 MHz, DMSO-d_6) δ 1070.29. HR-MS (+): *m*/*z* calculated mass for $(M + H)^+$ 976.3199, found 977.32 $[M + H]^+$. Analytical HPLC (5 to 60% MeCN/H_2O with 0.01% FA, v/v, 15 min): t_R = 9.70 min, purity = 97%. Elem. anal. calcd (%) for $C_{29}H_{58}Cl_2N_8O_{12}Pt$: C, 35.66; H, 5.99; N, 11.47. Found: C, 35.96; H, 5.68; N, 11.17.

[1*R*,2*R*-Cyclohexane-1,2-diamine](ethanedioato-*O*,*O*′) hydroxido-platinum-deferoxamine succinate (B). 0.05 g of **2** (0.066 mmol) were dissolved in 4 mL of DMSO and the solution was added dropwise to a suspension of [1*R*,2*R*-cyclohexane-1,2-diamine](ethanedioato-*O*,*O*′) hydroxido-platinum (0.030 g, 0.069 mmol) in 1 mL of DMSO. The solution was stirred at r.t. for 48 h in the dark at 40 °C, resulting in a light-yellow suspension. After filtration through cotton wool, the DMSO was evaporated by lyophilization and the residue was washed with methanol (2 × 5 mL), CH_2Cl_2 (5 mL) and diethyl ether (2 × 5 mL) and dried under reduced pressure. The residue was purified *via* gradient preparative PR-HPLC (C18 X-bridge) using (MeOH/H_2O with 0.1% TFA): 0–2 min (20% MeOH), 2–22 min (20–70% MeOH), 22–24 min (95% MeOH), 24–26 min (20% MeOH); the product eluted at 14.66 min, affording the pure compound as a pale-yellow powder (yield: 0.015 g, 20%). ^{1}H NMR (500 MHz, DMSO-d_6) δ 9.65 (s, 1H, $H_3CCONOH$), 9.60 (s, 2H, $COONOH$), 8.44 (d, J_{N-H} = 42.1 Hz, 2H, NH_2), 8.13–8.00 (m, 1H, NH_2), 7.86–7.82 (m, 1H, NH_2), 7.81–7.71 (m, 3H, NH), 3.45 (t, J = 6.9 Hz, 6H, $HONCH_2$), 3.00 (q, J = 6.4 Hz, 6H, $HNCH_2$), 2.57 (t, J = 6.8 Hz, 4H, $HONCOCH_2$ and 2H $CHNH_2$–Pt), 2.41 (t, J = 7.1 Hz, 2H, CH_2COOH), 2.36–2.19 (m, 6H, $HNCOCH_2$), 1.96 (s, 3H, CH_3), 1.54–1.42 (m, 10H, $HONCH_2CH_2$ and $CH_2CH_2CHNH_2$–Pt), 1.43.1.33 (m, 6H, $HNCH_2CH_2$), 1.26–1.10 (m, 8H, $HNCH_2CH_2CH_2$ and $CH_2CH_2CHNH_2$–Pt). ^{13}C NMR (125 MHz, DMSO-d_6) δ 181.29 (COO–Pt), 171.96 (HONCO), 171.31 ($HNCO_{succ}$), 171.20 (COHN), 170.14 ($COCH_3$), 163.90 and 163.86 (CO oxalate), 61.10 and 60.05 (Pt–NH_2CH), 47.10 and 46.79 ($HONCH_2$), 38.42 ($HNCH_2$), 32.21 (Pt–NH_2CHCH_2) and 31.33 (CH_2COO–Pt), 30.70 (CH_2CH_2COO–Pt), 29.92 (CH_2CONH), 28.82 ($HNCH_2CH_2$), 27.58 ($HONCOCH_2$), 26.03 ($HONCH_2CH_2$ and CH_2COO), 23.72 and 23.56 (Pt–$NH_2CHCH_2CH_2$), 23.50 ($HNCH_2CH_2CH_2$), 20.35 (CH_3). ^{195}Pt{^{1}H} NMR (108 MHz, DMSO-d_6) δ 1412.21. HR-MS (+): *m*/*z* calculated mass for $(M + H)^+$ 1074.42, found 1074.43 $[M + H]^+$. Analytical HPLC (5 to 60% MeCN/H_2O with 0.01% FA, v/v, 15 min): t_R = 10.00 min, purity = 98%. Elem. anal. calcd (%) for $C_{37}H_{66}N_8O_{16}Pt$: C, 41.38; H, 6.19; N, 10.43. Found: C, 41.71; H, 6.38; N, 10.83.

***cis*,*cis*,*trans*-[Pt(NH$_3$)$_2$Cl$_2$(CO$_2$C$_6$H$_5$)OH] (oxoplatin-monocarboxylate) (4).** 0.1 g of benzoic anhydride (0.440 mmol) were added to a suspension containing *cis*,*cis*,*trans*-$[Pt(NH_3)_2Cl_2(OH)_2]$ (0.1 g, 0.3 mmol) in DMSO (20 mL). The reaction was stirred at r.t. for 12 h and then was filtered to remove unreacted starting materials. The filtrate was lyophilized and washed with acetone (3 × 10 mL), cold dichloromethane (1 × 5 mL) and methanol (3 × 10 mL) and dried under reduced pressure to yield the product as a white precipitate (yield: 0.094 g, 74%). ^{1}H NMR (500 MHz, DMSO-d_6) δ 7.88 (d, J = 7.8 Hz, 2H, H_A), 7.48 (t, J = 7.8 Hz, 1H, H_C), 7.40 (t, J = 7.5 Hz, 2H, H_B), 6.07 (m, J_{H-N} = 52.98 Hz, J_{H-Pt} = 52.9 Hz, 6H, NH_3). ^{13}C NMR (126 MHz, DMSO-d_6) δ 173.52 (CO), 134.79 (C_C), 131.12 (C_D), 129.36 (C_A), 127.75 (C_B). ^{195}Pt{^{1}H} NMR (108 MHz, DMSO-d_6) δ 2040.20.

***cis*,*cis*,*trans*-[Pt(NH$_3$)$_2$Cl$_2$(CO$_2$C$_6$H$_5$)CO$_2$C$_2$H$_4$COOH] (5).** 0.05 g of **3** (0.114 mmol) and succinic anhydride (0.07 g, 0.700 mmol) were dissolved in 10 ml of DMSO and stirred at 50 °C for 24 h. The reaction mixture was lyophilized and washed with dichloromethane (3 × 5 ml) and dried under reduced pressure, obtaining a white powder which was used without further purification. (yield: 0.056 g, 91%). ^{1}H NMR (500 MHz, DMSO-d_6) δ 12.12 (s, 1H $COOH$), 7.87 (d, J = 7.0 Hz, 2H, H_A), 7.52 (t, J = 7.4 Hz, 1H, H_C), 7.42 (t, J = 7.6 Hz, 2H, H_B), 6.62 (m, 6H, NH_3–Pt), 2.53 (t, J = 7.1 Hz, 2H, CH_2COOH), 2.40 (t, J = 7.3 Hz, 2H, CH_2COO–Pt). ^{13}C NMR (126 MHz, DMSO-d_6) δ 179.70 (COOH), 173.92 (COO–Pt), 173.44 (CO), 133.16 (C_C), 131.77 (C_D), 129.44 (C_A), 127.99 (C_B), 30.48 (CH_2), 29.91 (CH_2). ^{195}Pt{^{1}H} NMR (108 MHz, DMSO-d_6) δ 1211.93.

***cis*,*cis*,*trans*-[Pt(NH$_3$)$_2$Cl$_2$(CO$_2$C$_6$H$_5$)CO$_2$C$_2$H$_4$COO-deferoxamine] (C).** 0.06 g of **4** (0.056 mmol) were dissolved in 2.5 ml of dry DMF and placed under nitrogen atmosphere. 0.044 g TBTU were added to the solution, followed by 24 μL of DIPEA. The suspension was stirred for 10 min and then was added dropwise to a suspension containing 0.088 g (0.067 mmol) of DFOM and 24 μL of DIPEA in 2.5 ml of dry DMF. The reaction mixture was stirred at 35 °C for 16 h. The solvent was removed by rotary evaporation, obtaining a yellow oil which was triturated with10 ml of cold dichloromethane and 10 mL of diethyl ether obtaining 0.12 g of a light-yellow powder. The residue was purified *via* gradient preparative PR-HPLC (C18 X-bridge) using (MeCN/H_2O with 0.1% TFA): 0–2 min (5% MeCN),

2–21 min (5–40% MeCN), 21–23 min (95% MeCN), 23–25 min (5% MeCN); the product eluted at 19.9 min, affording the pure compound as a pale-yellow powder (yield: 0.021 g, 35%). ^{1}H NMR (500 MHz, DMSO-d_6) δ 9.63 (d, J = 20.4 Hz, 3H, $H_3CCONOH$), 7.88 (d, J = 7.0 Hz, 2H, H_A), 7.82 (t, J = 5.5 Hz, 1H, NH), 7.77 (t, J = 5.0 Hz, 2H, NH), 7.82 (t, J = 5.5 Hz, 1H, H_C), 7.77 (t, J = 5.0 Hz, 2H, H_B), 6.80–6.44 (m, 6H, NH_3-Pt), 3.45 (t, 6H, HONCH_2), 3.00 (q, J = 7.1 Hz, 6H, HNCH_2), 2.57 (t, J = 7.1 Hz, 4H, HONCOCH_2), 2.47 (t, J = 7.5 Hz, 2H, CH_2COOH), 2.28 (dt, J = 11.8, 7.4 Hz, 6H, HNCOCH_2), 1.96 (s, 3H CH_3), 1.54–1.45 (m, 6H, HONCH_2CH_2), 1.43–1.32 (m, 6H, HNCH_2CH_2), 1.26–1.13 (m, 6H, HNCH_2CH_2CH_2). ^{13}C NMR (126 MHz, DMSO-d_6) δ 180.09 (COO–Pt), 173.33 (CO_{Benz}), 171.99 (HONCO), 171.34 (HNCOsucc), 171.23 (CONH), 170.16 (CH_3CO), 133.15 (C_C), 131.67 (C_D), 129.38 (C_A), 127.91 (C_B), 47.10 and 46.80 (HONCH_2), 38.49 and 38.44 (HNCH_2), 31.46 (CH_2COO–Pt), 31.35 (CH_2CH_2COO–Pt), 29.91 (CH_2CONH), 28.82 (HNCH_2CH_2), 27.58 (HONCOCH_2), 26.04 (HONCH_2CH_2), 23.56 and 23.51 (HNCH_2CH_2CH_2), 20.36 (CH_3). ^{195}Pt{^{1}H} NMR (108 MHz, DMSO-d_6) δ 1210.30. HR-MS (+): m/z calculated mass for $(M + H)^+$ 1080.92, found 1103.3 $[M + Na]^+$. Analytical HPLC (5 to 60% MeCN/H_2O with 0.01% FA, v/v, 15 min): t_R = 12.58 min, purity = 95%. Elem. anal. calcd (%) for $C_{36}H_{62}Cl_2N_8O_{13}Pt$: C, 40.00; H, 5.78; N, 10.37. Found: C, 40.39; H, 5.37; N, 10.7.

Conclusions

Three novel Pt(IV) complexes **A**, **B** and **C** functionalized with a DFO chelator for radiolabeling applications were synthesized and characterized as potential theranostic agents. All complexes demonstrated stability in physiological conditions. Their prodrug nature was confirmed by reduction studies in the presence of ascorbic acid and in Cyclic Voltammetry. Further biological evaluation revealed that none of the complexes were toxic towards healthy MDCK.2 canine kidney cells, underscoring their reduced nephrotoxicity compared to cisplatin. Moreover, cellular uptake experiments in osteosarcoma cell lines demonstrated that complex **C** is better internalized, followed by complex **A** and cisplatin, consistent with its higher lipophilicity (log D). Finally, all three complexes were successfully radiolabeled with ^{68}Ga, achieving quantitative incorporation, high radiochemical purities (94–97%) and stability in PBS and human blood serum after 1 h. Their robust radiolabeling, combined with stability and minimal nephrotoxicity, makes them attractive candidates for *in vivo* PET imaging studies. While their cytotoxicity against the osteosarcoma cell lines U2OS and 143B is lower than cisplatin, which was anticipated from the hydrophilic axial ligand (DFO), it does not diminish their value as theranostic agents. Instead, these compounds provide an example of prodrugs that can be radiolabeled to enable real-time, non-invasive biodistribution and tumor-uptake studies. Together with the potential for ^{68}Ga labeling, these results highlight their strong promise as theranostic agents that bridge platinum chemotherapy with molecular imaging. While the present work focuses on the *in vitro* characterization and radiochemical feasibility of Pt(IV)–DFO conjugates, future studies will aim to assess their *in vivo* biodistribution and pharmacokinetic properties through ^{68}Ga PET imaging to further establish their theranostic potential. Different chelating ligands such as HBED CC (*N*,*N*′-bis(2-hydroxy-5-(carboxyethyl)benzyl)ethylenediamine-*N*,*N*′-diacetic acid), NOTA (1,4,7-triazacyclononane-1,4,7-triacetic acid) and THP (hexadentate tris(3,4-hydroxypyridinone)) will be considered as alternative to DFO in the synthesis of Pt(IV) complexes due to their very promising radiolabeling properties.

Author contributions

G. F., I. L. M. and M. S.: investigation, formal analysis, visualization, writing – original draft, writing – review & editing. E. D.: data curation, supervision. T. W. and S. P.: data curation, visualization, supervision, project administration, writing – review & editing. I. P.-M.: supervision, resources, writing – review & editing. M. H.: resources. C. K.: data curation, visualization, project administration, funding acquisition, supervision. M. M.: conceptualization, data curation, funding acquisition, project administration, supervision, visualization, writing – review & editing. D. M.: conceptualization, data curation, funding acquisition, project administration, supervision, visualization, writing – original draft, writing – review & editing. All authors have read and agreed to the published version of the manuscript.

Conflicts of interest

There are no conflicts to declare.

Data availability

The data supporting this article have been included as part of the supplementary information (SI). Supplementary information is available. See DOI: https://doi.org/10.1039/d5dt02352a.

Acknowledgements

This research was funded by the STRIKE project HORIZON-MSCA-2021-DN-01, grant number. 101072462. G. F. and D. M. thankfully acknowledge support from Science Foundation Ireland (SFI): SFI 2012 Strategic Opportunity Fund (Infrastructure award 12/RI/2346/SOF) for NMR facilities. SFI Opportunistic Infrastructure Fund 2016 (16/RI/3399) for LC-MS. Dr Maria Galiana Cameo is acknowledged for her preliminary contribution on DFO activation. We especially want to thank Marie Brandt, Marius Ozenil, and Karsten Bamminger for their support in establishing the radiolabeling procedure.

References

1 N. J. Wheate, *et al.*, *Dalton Trans.*, 2010, **39**, 8113–8127, DOI: 10.1039/C0DT00292E.
2 B. Das, S. Sathyanarayan and P. Gupta, *Dalton Trans.*, 2025, **54**, 10178–10206, DOI: 10.1039/D5DT00678C.
3 F. Castro, *et al.*, *Coord. Chem. Rev.*, 2022, **451**, 214276, DOI: 10.1016/j.ccr.2021.214276.
4 T. C. Johnstone, K. Suntharalingam and S. J. Lippard, *Chem. Rev.*, 2016, **116**, 3436, DOI: 10.1021/acs.chemrev.5b00597.
5 D. Gibson, *J. Inorg. Biochem.*, 2019, **191**, 77–84, DOI: 10.1016/j.jinorgbio.2018.11.008.
6 R. G. Kenny and C. J. Marmion, *Chem. Rev.*, 2019, **119**, 1058–1137, DOI: 10.1021/acs.chemrev.8b00271.
7 E. Gabano, M. Ravera and D. Osella, *Dalton Trans.*, 2014, **43**, 9813–9820, DOI: 10.1039/C4DT00911H.
8 G. Ferrari, I. Lopez-Martinez, *et al.*, *Molecules*, 2024, **29**(15), 3453, DOI: 10.3390/molecules29153453.
9 S. Entezari, *et al.*, *J. Toxicol.*, 2022, 4911205, DOI: 10.1155/2022/4911205.
10 T. E. Wuensche, *et al.*, *EJNMMI Radiopharm. Chem.*, 2024, **9**(40), DOI: 10.1186/s41181-024-00258-y.
11 P. G. Casali, *et al.*, *Ann. Oncol.*, 2018, **29**, iv51–iv67, DOI: 10.1093/annonc/mdy096.
12 D. Heymann, *Bone Sarcomas and Bone Metastases - From Bench to Bedside*. Academic Press, 2021.
13 E. S. Kleinerman and R. Gorlick, *Current Advances in Osteosarcoma Clinical Perspectives: Past, Present and Future*, Springer, 2020.
14 L. Mirabello, R. J. Troisi and S. A. Savage, *Cancer*, 2009, **115**(7), 1531–1543, DOI: 10.1002/cncr.24121.
15 F. Liu, *et al.*, *BMC Cancer*, 2019, **19**, 323, DOI: 10.1186/s12885-019-5488-5.
16 C. Oh, *et al.*, *J. Nucl. Med.*, 2023, **64**(6), 842–851, DOI: 10.2967/jnumed.123.265592.
17 S. A. Koerber, *et al.*, *Eur. J. Nucl. Med. Mol. Imaging*, 2021, **48**, 3918–3924, DOI: 10.1007/s00259-021-05374-4.
18 C. Imberti, *et al.*, *Inorg. Chem.*, 2023, **62**(50), 20745–20753, DOI: 10.1021/acs.inorgchem.3c02245.
19 S. Harringer, *et al.*, *Dalton Trans.*, 2021, **50**, 8167–8178, DOI: 10.1039/D1DT00214G.
20 M. Kraihammer, *et al.*, *Eur. J. Med. Chem.*, 2026, **301**, 118216, DOI: 10.1016/j.ejmech.2025.118216.
21 D. F. Beirne, *et al.*, *Dalton Trans.*, 2023, **52**, 14110–14122, DOI: 10.1039/D3DT02030D.
22 E. Moynihan, *et al.*, *Front. Chem.*, 2021, **9**, 795997, DOI: 10.3389/fchem.2021.79599.
23 J. E. Baldwin, *J. Chem. Soc., Chem. Commun.*, 1976, 734–736.
24 C. F. Chin, *et al.*, *Chem. Sci.*, 2014, **5**, 2265–2270, DOI: 10.1039/C3SC53106F.
25 S. Chen, *et al.*, *Dalton Trans.*, 2022, **51**, 885–897, DOI: 10.1039/D1DT03959H.
26 J. Z. Zhang, *et al.*, *Chem. Commun.*, 2012, **48**, 847–849, DOI: 10.1039/C1CC16647F.
27 R. Darabi, M. Shabani-Nooshabadi and A. Khoobi, *J. Electrochem. Soc.*, 2021, **168**, 046514, DOI: 10.1149/1945-7111/abf6ed.
28 S. Choi, *et al.*, *Inorg. Chem.*, 1998, **37**(10), 2500–2504.
29 T. Ludwig, *et al.*, *Kidney Int.*, 2004, **66**(1), 196–202.
30 C. Tang, *et al.*, *Nat. Rev. Nephrol.*, 2023, **19**(1), 53–72, DOI: 10.1038/s41581-022-00631-7.
31 S. U. Lauvrak, *et al.*, *Br. J. Cancer*, 2013, **109**(8), 2228–2236, DOI: 10.1038/bjc.2013.549.
32 Y. Liu, *et al.*, *J. Orthop. Res.*, 2016, **34**(12), 2116–2125, DOI: 10.1002/jor.23245.
33 S. Dhara, *Indian J. Chem.*, 1970, **8**, 193.
34 R. J. Brandon and J. C. Dabrowiak, *J. Med. Chem.*, 1984, **27**(7), 861–865, DOI: 10.1021/jm00373a009.